

**Inclusive electron scattering off  $^4\text{He}$** Sonia Bacca,<sup>1,\*</sup> Hartmuth Arenhövel,<sup>2</sup> Nir Barnea,<sup>3</sup> Winfried Leidemann,<sup>4</sup> and Giuseppina Orlandini<sup>4</sup><sup>1</sup>*Gesellschaft für Schwerionenforschung, Planckstr. 1, D-64291 Darmstadt, Germany*<sup>2</sup>*Institut für Kernphysik, Johannes Gutenberg-Universität, J.J.-Becher-Weg 45, D-55099 Mainz, Germany*<sup>3</sup>*Racah Institute of Physics, Hebrew University, 91904, Jerusalem, Israel*<sup>4</sup>*Dipartimento di Fisica, Università di Trento and INFN (Gruppo Collegato di Trento), via Sommarive 14, I-38100 Trento, Italy*

(Received 8 March 2007; published 18 July 2007)

Inclusive electron scattering off  $^4\text{He}$  is investigated for low and medium energy and momentum transfers. The final state interaction, given by the simple semirealistic Malfliet-Tjon potential, is treated rigorously applying the Lorentz integral transform (LIT) method. In addition to the nonrelativistic one-body current a consistent meson exchange current is constructed and implemented. Results are presented for both longitudinal and transverse response functions at various momentum transfers. Good agreement with experimental data is found for the longitudinal response function, whereas some strength is missing in the transverse response function on the low energy side of the quasi-elastic peak.

DOI: [10.1103/PhysRevC.76.014003](https://doi.org/10.1103/PhysRevC.76.014003)

PACS number(s): 25.30.Fj, 21.45.+v, 27.10.+h, 31.15.Ja

**I. INTRODUCTION**

In recent years considerable progress has been achieved in rigorous microscopic nuclear structure calculations of few-body nuclei with realistic or at least semirealistic interactions. Quite different approaches have been devised for bound-state problems (see Ref. [1]). For breakup observables the powerful method of the Lorentz integral transform (LIT) has been developed in Ref. [2]. The method is very convenient for calculating cross sections of perturbation-induced reactions, where the inelastic response of the nuclear system is given by an absolute square of a transition matrix element summed over the whole spectrum of final states. Within this approach one does not evaluate the response function straightforwardly but calculates instead an integral transform of the response with a Lorentzian kernel. The response function itself is then obtained by inverting the transform. The specific advantage of this method lies in the fact that no explicit calculation of the complicated spectrum of final state wave functions is required.

Over recent years, the LIT method has been exploited very successfully in the calculation of electromagnetic inclusive responses of various light nuclei (see, e.g., Refs. [3–5]), of neutrino inelastic reactions [6,7], and even of exclusive processes (see, e.g., Refs. [8,9]). With respect to inclusive electron scattering considered here, until now only the longitudinal response function  $R_L$ , induced by the electromagnetic charge  $\rho(\mathbf{q})$ , has been investigated in the LIT approach, namely for  $^3\text{H}$  and  $^3\text{He}$  with realistic nuclear forces [10,11] and for  $^4\text{He}$  with the semirealistic TN potential [12,13], whereas the transverse response  $R_T$ , induced by the current density operator  $\mathbf{j}(\mathbf{q})$ , has not yet been considered within this method.

In the present work we evaluate both inclusive responses of the four-body system  $^4\text{He}$ . With the exception of Refs. [12,13], most previous calculations of  $R_L$  and  $R_T$  relied on the plane wave impulse approximation (PWIA) (see, e.g., Ref. [14]), where the interaction among the final reaction products is

neglected (PW) and where only one-body electromagnetic operators are considered (IA). In Ref. [15,16] the Laplace transforms of the two responses (the so-called Euclidean responses) were calculated using the Green function Monte Carlo (GFMC) method with a realistic interaction and a consistent treatment of additional meson exchange currents (MEC). This work showed that (i) the final-state interaction (FSI) is relevant in light nuclei, especially in the longitudinal response, and (ii) two-body currents are important in the reaction mechanism, because they were found to have an enhancing effect of about 20% on the Euclidean transverse response. The strong FSI effect on  $R_L$  of  $^4\text{He}$  was confirmed in the above-mentioned LIT calculation [12,13] with a semirealistic force, where reliable results were obtained not only for a transform of  $R_L$ , but also for  $R_L$  itself.

The main aim of the present work is the calculation of  $R_T$  for  $^4\text{He}$  with a complete treatment of the final-state interaction and using a current that is consistent with the potential. Because it is the first calculation using the LIT method we have chosen a semirealistic potential, i.e., the Malfliet-Tjon potential [17]. The longitudinal response function of  $^4\text{He}$  will be reconsidered with this potential as well. In our calculation the final-state interaction of the four-body continuum is fully taken into account via the LIT method. Compared to the Laplace transform, the use of a Lorentz kernel has the advantage that a stable inversion of the integral transform is possible, thus allowing a direct comparison of the theoretical predictions with experimental data.

In the following section we give a brief theoretical overview of the LIT method and remind the reader of the definition of the inclusive electron scattering response functions. Then in Sec. III we discuss our results for the longitudinal and transverse response functions, and in the last section we draw some conclusions and give an outlook.

**II. THEORETICAL FRAMEWORK**

In this section we outline the main theoretical concepts for the present calculation of the electromagnetic response

\*s.bacca@gsi.de

functions that govern the inclusive electron scattering off nuclei. First, we give a short account of the Lorentz integral transform (LIT) that allows one to calculate the response functions with complete inclusion of the nuclear interaction in the final states. Then, in the second part, we briefly review the definition of the electromagnetic response functions and the model of the nuclear one- and two-body currents.

### A. The Lorentz integral transform

As already mentioned, the basic observable is a response function that in the laboratory system has the general form

$$R_{\mathcal{O}}(\omega, \mathbf{q}) = \sum_f |\langle \Psi_f | \mathcal{O}(\mathbf{q}) | \Psi_0 \rangle|^2 \times \delta \left( E_f + \frac{\mathbf{q}^2}{2M} - E_0 - \omega \right), \quad (1)$$

where  $M$  is the target mass and  $|\Psi_{0/f}\rangle$  and  $E_{0/f}$  denote initial- and final-state wave functions and energies, respectively, whereas  $\omega$  and  $\mathbf{q}$  are the energy and momentum transfers. The operator  $\mathcal{O}$ , describing the perturbative excitation mechanism, will be specified in the following subsection. The  $\delta$  function ensures energy conservation. The response function includes a sum over all possible final states, which are excited by the electromagnetic probe. This includes also the scattering states in the continuum. Therefore, in a straightforward evaluation one would need to calculate in addition to the initial ground state the final excited bound and continuum states of which the latter constitute the major obstacle for a many-body nucleus if one wants to include the nuclear interaction rigorously.

In the LIT method [2] this difficulty is circumvented by considering instead of the response function  $R_{\mathcal{O}}(\omega, \mathbf{q})$  an integral transform  $L_{\mathcal{O}}(\sigma, \mathbf{q})$  with a Lorentzian kernel defined for a complex parameter  $\sigma = \sigma_R + i\sigma_I$  by

$$L_{\mathcal{O}}(\sigma, \mathbf{q}) = \int d\omega \frac{R_{\mathcal{O}}(\omega, \mathbf{q})}{(\omega - \sigma_R)^2 + \sigma_I^2}. \quad (2)$$

The imaginary part of  $\sigma$  is kept at a constant finite value ( $\sigma_I \neq 0$ ) determining the resolution of the integral transform. The basic idea of considering the integral transform is that it can be evaluated from the norm of a state  $|\tilde{\Psi}_{\sigma, \mathbf{q}}^{\mathcal{O}}\rangle$ , i.e.,

$$L_{\mathcal{O}}(\sigma, \mathbf{q}) = \left\langle \tilde{\Psi}_{\sigma, \mathbf{q}}^{\mathcal{O}} \left| \tilde{\Psi}_{\sigma, \mathbf{q}}^{\mathcal{O}} \right. \right\rangle, \quad (3)$$

where  $|\tilde{\Psi}_{\sigma, \mathbf{q}}^{\mathcal{O}}\rangle$  is the unique solution of the inhomogeneous “Schrödinger-like” equation

$$(H - E_0 - \sigma) \left| \tilde{\Psi}_{\sigma, \mathbf{q}}^{\mathcal{O}} \right\rangle = \mathcal{O}(\mathbf{q}) |\Psi_0\rangle. \quad (4)$$

Here  $H$  denotes the nuclear Hamiltonian. Because of the presence of a nonvanishing imaginary part  $\sigma_I$  in Eq. (4) and the fact that its right-hand side is localized, one has an asymptotic boundary condition as for a bound state. Thus, one can apply bound-state techniques for its solution. The response function itself, as a function of the energy  $\omega$  for fixed  $\mathbf{q}$ , is then obtained by inverting the integral transform (2) for which various methods have been devised [18,19].

### B. The response functions of electron scattering

In the one-photon-exchange approximation, the inclusive cross section for electron scattering off a nucleus is given in terms of two response functions, i.e.,

$$\frac{d^2\sigma}{d\Omega d\omega} = \sigma_M \left[ \frac{Q^4}{q^4} R_L(\omega, \mathbf{q}) + \left( \frac{Q^2}{2q^2} + \tan^2 \frac{\theta}{2} \right) R_T(\omega, \mathbf{q}) \right], \quad (5)$$

where  $\sigma_M$  denotes the Mott cross section,  $Q^2 = -q_\mu^2 = \mathbf{q}^2 - \omega^2$  the squared four-momentum transfer with  $\omega$  and  $\mathbf{q}$  as energy and three-momentum transfers, respectively, and  $\theta$  the scattering angle. The longitudinal and transverse response functions,  $R_L(\omega, \mathbf{q})$  and  $R_T(\omega, \mathbf{q})$ , are determined by the transition matrix elements of the Fourier transforms of the charge and the transverse current density operators,  $\rho(\mathbf{q})$  and  $\mathbf{j}_T(\mathbf{q})$ , respectively,

$$R_L(\omega, \mathbf{q}) = \sum_f |\langle \Psi_f | \rho(\mathbf{q}) | \Psi_0 \rangle|^2 \times \delta \left( E_f + \frac{\mathbf{q}^2}{2M} - E_0 - \omega \right), \quad (6)$$

$$R_T(\omega, \mathbf{q}) = \sum_f |\langle \Psi_f | \mathbf{j}_T(\mathbf{q}) | \Psi_0 \rangle|^2 \times \delta \left( E_f + \frac{\mathbf{q}^2}{2M} - E_0 - \omega \right). \quad (7)$$

#### 1. Multipole expansion

It is useful to decompose the charge and current densities into Coulomb, longitudinal, and transverse electric and magnetic multipoles [20]

$$\rho(\mathbf{q}) = 4\pi \sum_{J\mu} C_\mu^J(\mathbf{q}) Y_\mu^J(\hat{\mathbf{q}})^*, \quad (8)$$

$$\mathbf{j}(\mathbf{q}) = \sum_{J\mu} \sqrt{4\pi} \hat{\mathbf{j}} \left\{ L_\mu^J(\mathbf{q}) \mathbf{e}_0 - \frac{1}{\sqrt{2}} [T_\mu^{el,J}(\mathbf{q}) + \mu T_\mu^{\text{mag},J}(\mathbf{q})] \mathbf{e}_\mu^* \right\}, \quad (9)$$

where  $\{\mathbf{e}_\mu; \mu = 0, \pm 1\}$  is a set of orthogonal spherical unit vectors with  $\mathbf{e}_0$  along  $\mathbf{q}$ . Here the Coulomb and transverse multipole operators are defined as

$$C_\mu^J(\mathbf{q}) = \frac{1}{4\pi} \int d\hat{\mathbf{q}}' \tilde{\rho}(\mathbf{q}') Y_\mu^J(\hat{\mathbf{q}}'), \quad (10)$$

$$L_\mu^J(\mathbf{q}) = \frac{i}{4\pi} \int d\hat{\mathbf{q}}' [\hat{\mathbf{q}}' \cdot \mathbf{j}(\mathbf{q}')] Y_\mu^J(\hat{\mathbf{q}}'), \quad (11)$$

$$T_\mu^{el,J}(\mathbf{q}) = \frac{i}{4\pi} \int d\hat{\mathbf{q}}' [\hat{\mathbf{q}}' \times \mathbf{Y}_{J\mu}^J(\hat{\mathbf{q}}')] \cdot \mathbf{j}(\mathbf{q}'), \quad (12)$$

$$T_\mu^{\text{mag},J}(\mathbf{q}) = \frac{1}{4\pi} \int d\hat{\mathbf{q}}' \mathbf{j}(\mathbf{q}') \cdot \mathbf{Y}_{J\mu}^J(\hat{\mathbf{q}}'). \quad (13)$$

Coulomb and longitudinal multipoles are related via current conservation, i.e.,

$$L_\mu^J(q) = \frac{i}{q} [H, C_\mu^J(q)]. \quad (14)$$

## 2. Siegert theorem and Siegert operators

As is well known, the Siegert theorem states that in the low energy limit the transverse electric multipoles are related to the Coulomb multipoles. This is a very important and also very useful theorem, because it enables one to calculate, in the low energy regime, electric transition matrix elements from the charge density, without explicit knowledge of the current operator.

Even beyond the low energy regime, one can always write each electric multipole as a sum of a Siegert operator plus a correction term. This is achieved by casting the transverse electric multipole operator in Eq. (12) into the form

$$\begin{aligned} T_\mu^{el,J}(q) &= -\frac{1}{4\pi} \int d\hat{q}' \left\{ \sqrt{\frac{J+1}{J}} [\hat{q}' \cdot \mathbf{j}(q')] Y_\mu^J(\hat{q}') \right. \\ &\quad \left. + \frac{\hat{J}}{\sqrt{J}} Y_{J+1,\mu}^J(\hat{q}') \cdot \mathbf{j}(q') \right\} \\ &= S_\mu^J(q) + K_\mu^J(q), \end{aligned} \quad (15)$$

where the first term is related to the the longitudinal multipole operator (see Eq. (11))

$$\begin{aligned} S_\mu^J(q) &= -\frac{1}{4\pi} \sqrt{\frac{J+1}{J}} \int d\hat{q}' (\hat{q}' \cdot \mathbf{j}(q')) Y_\mu^J(\hat{q}') \\ &= i \sqrt{\frac{J+1}{J}} L_\mu^J(q) \end{aligned} \quad (16)$$

and

$$K_\mu^J(q) = -\frac{1}{4\pi} \frac{\hat{J}}{\sqrt{J}} \int d\hat{q}' Y_{J+1,\mu}^J(\hat{q}') \cdot \mathbf{j}(q'). \quad (17)$$

Using the relation (14) from current conservation, the first term can be expressed by the Coulomb operator of Eq. (10), yielding

$$S_\mu^J(q) = -\frac{1}{q} \sqrt{\frac{J+1}{J}} [H, C_\mu^J(q)]. \quad (18)$$

This form of  $S_\mu^J(q)$  is called the *Siegert operator*. As is often said, the advantage of the Siegert operator is that, if evaluated with the one-body charge density, it already includes the dominant part of the MEC. The additional term  $K_\mu^J(q)$  is a correction to the Siegert operator, and in the limit that the photon momentum goes to zero, the Siegert operator dominates the electric multipole, because the correction  $K_\mu^J(q)$  is two orders in  $q$  higher. Therefore, the approximation of the transverse electric multipoles by the Siegert operators is quite reliable at low photon momentum, i.e., for  $qR \ll 1$ , where  $R$  characterizes the spatial extension of the system. However, with increasing  $q$ , one has to calculate also the contribution of  $K_\mu^J(q)$ , which requires the knowledge of the explicit form of the current operator.

## 3. The current density operators

In general, the electromagnetic current density of a nucleus can be decomposed in a superposition of one- and many-body operators. In a nonrelativistic approach, as is the case here, the electromagnetic one-body four-current is given by the free nucleon current density operator, i.e.,

$$\rho_{(1)}(\mathbf{x}) = \frac{e}{2} \sum_k (1 + \tau_k^3) \delta(\mathbf{x} - \mathbf{r}_k), \quad (19)$$

for the charge density, where  $\tau_k^3$  is the third component of the isospin of the “ $k$ -th” particle. The current density consists of a convection and a spin current

$$\mathbf{j}_{(1)}(\mathbf{x}) = \mathbf{j}_{(1)}^c(\mathbf{x}) + \mathbf{j}_{(1)}^s(\mathbf{x}), \quad (20)$$

with

$$\begin{aligned} \mathbf{j}_{(1)}^c(\mathbf{x}) &= \frac{e}{4m} \sum_k (1 + \tau_k^3) \{ \mathbf{p}_k, \delta(\mathbf{x} - \mathbf{r}_k) \}, \\ \mathbf{j}_{(1)}^s(\mathbf{x}) &= i \frac{e}{2m} \sum_k (\mu^s + \tau_k^3 \mu^v) \boldsymbol{\sigma}_k \times [\mathbf{p}_k, \delta(\mathbf{x} - \mathbf{r}_k)], \end{aligned} \quad (21)$$

where  $\mu^s, \mu^v, \boldsymbol{\sigma}_k, \mathbf{p}_k$ , and  $m$  denote isoscalar and isovector nucleon magnetic moments, spin, momentum, and mass of the “ $k$ -th” particle, respectively. These expressions describe point particles. To take into account the internal nucleon structure, charge and magnetic moments have to be replaced by the corresponding form factors

$$\begin{aligned} \frac{1}{2}(1 + \tau_k^3) &\rightarrow G_E^s(Q^2) + \tau_k^3 G_E^v(Q^2), \\ \mu^s + \mu^v \tau_k^3 &\rightarrow G_M^s(Q^2) + \tau_k^3 G_M^v(Q^2). \end{aligned} \quad (22)$$

For on-shell particles, these form factors depend on the squared four-momentum transfer  $Q^2$  alone. In principle, this is no longer true for the off-shell situation. However, in view of the fact that little is known about the off-shell continuation and furthermore for the moderate energy and momentum transfers considered here, the neglect of such effects is justified. Here we use for all form factors a common dependence on  $Q^2$  of the usual dipole form [21].

To satisfy the continuity equation

$$\nabla \cdot \mathbf{j}_{(2)}(\mathbf{x}) = -i[V, \rho_{(1)}(\mathbf{x})]. \quad (23)$$

a momentum- and/or isospin-dependent two-body interaction  $V$  requires a two-body current density operator, the interaction (or meson exchange) current. As is well known, relation (23) is not sufficient to determine the two-body current uniquely. Therefore one needs in principle a dynamic model for the nuclear potential that reveals the underlying interaction mechanism. Such a model is supplied by the meson exchange picture of the  $NN$  interaction. But even for a phenomenological potential often a consistent MEC can be constructed if the potential has the formal appearance of a meson-exchange potential. This is achieved using the method developed independently in Refs. [22] and [23]. The method is based on the observation that if a potential is given as a sum of Yukawa-like terms, one can interpret the potential as produced by the exchange of fictitious mesons whose exchange currents

are known. In the present case we use the semirealistic Malfliet-Tjon potential [17], which is isospin dependent and thus requires a MEC. Despite its phenomenological character, it fulfills the just mentioned requirement and thus it is possible to derive a consistent MEC which satisfies (23) with this potential.

Explicitly, the MT potential has the form

$$V(r) = V_{13}(r)P_{13} + V_{31}(r)P_{31}, \quad (24)$$

where  $P_{13}$  and  $P_{31}$  denote the projectors on the spinsinglet-isotriplet and spintriplet-isosinglet two-nucleon states, respectively,

$$P_{13} = \frac{1}{16}(1 - \boldsymbol{\sigma}_1 \cdot \boldsymbol{\sigma}_2)(3 + \boldsymbol{\tau}_1 \cdot \boldsymbol{\tau}_2), \quad (25)$$

$$P_{31} = \frac{1}{16}(3 + \boldsymbol{\sigma}_1 \cdot \boldsymbol{\sigma}_2)(1 - \boldsymbol{\tau}_1 \cdot \boldsymbol{\tau}_2). \quad (26)$$

Furthermore, the radial functions are given by

$$V_{13}(r) = 4\pi[AJ_{m_1}(r) - BJ_{m_2}(r)], \quad (27)$$

$$V_{31}(r) = 4\pi[CJ_{m_1}(r) - DJ_{m_2}(r)], \quad (28)$$

with  $J_{m_{1/2}}(r) = e^{-m_{1/2}r}/4\pi r$ ,  $m_1 = 3.11 \text{ fm}^{-1}$ ,  $m_2 = 1.55 \text{ fm}^{-1}$  and  $A = C = 1458.047 \text{ MeV fm}$ ,  $B = 520.872 \text{ MeV fm}$ ,  $D = 635.306 \text{ MeV fm}$ . Exhibiting explicitly the spin-isospin dependence, one can rewrite the potential in the form

$$V(r) = V_0(r) + V_\sigma(r)\boldsymbol{\sigma}_1 \cdot \boldsymbol{\sigma}_2 + (V_\tau(r) + V_{\sigma\tau}(r)\boldsymbol{\sigma}_1 \cdot \boldsymbol{\sigma}_2)\boldsymbol{\tau}_1 \cdot \boldsymbol{\tau}_2, \quad (29)$$

with

$$V_0(r) = \frac{12\pi}{16}[AJ_{m_1}(r) - BJ_{m_2}(r) + CJ_{m_1}(r) - DJ_{m_2}(r)], \quad (30)$$

$$V_\sigma(r) = \frac{4\pi}{16}[-3AJ_{m_1}(r) + 3BJ_{m_2}(r) + CJ_{m_1}(r) - DJ_{m_2}(r)], \quad (31)$$

$$V_\tau(r) = \frac{4\pi}{16}[AJ_{m_1}(r) - BJ_{m_2}(r) - 3CJ_{m_1}(r) + 3DJ_{m_2}(r)], \quad (32)$$

$$V_{\sigma\tau}(r) = \frac{4\pi}{16}[-AJ_{m_1}(r) + BJ_{m_2}(r) - CJ_{m_1}(r) + DJ_{m_2}(r)]. \quad (33)$$

Because the isospin independent part commutes with the charge operator, only the isospin dependent part of (29) is relevant for the MEC. One can bring it into the form

$$V_\tau(r) + V_{\sigma\tau}(r) = 4\pi\boldsymbol{\tau}_1 \cdot \boldsymbol{\tau}_2\{\alpha J_{m_1}(r) + \beta J_{m_2}(r) + [\gamma J_{m_1}(r) + \delta J_{m_2}(r)]\boldsymbol{\sigma}_1 \cdot \boldsymbol{\sigma}_2\}, \quad (34)$$

where the new constants are defined as

$$\begin{aligned} \alpha &= \frac{1}{16}(A - 3C), & \beta &= -\frac{1}{16}(B - 3D), \\ \gamma &= -\frac{1}{16}(A + C), & \delta &= \frac{1}{16}(B + D). \end{aligned}$$

Now, because  $J_m(r)$  represents the propagator of an exchanged scalar meson of mass  $m$ , the corresponding meson exchange

current is easily constructed (for details see Ref. [24]) and one finds

$$\begin{aligned} \mathbf{j}_{(2)}^{\text{MTI-III}}(\mathbf{x}, \mathbf{r}_1, \mathbf{r}_2) &= 4\pi(\boldsymbol{\tau}_1 \times \boldsymbol{\tau}_2)_3[\alpha J_{m_1}(|\mathbf{r}_1 - \mathbf{x}|) \overleftrightarrow{\nabla}_x J_{m_1}(|\mathbf{x} - \mathbf{r}_2|) \\ &+ \beta J_{m_2}(|\mathbf{r}_1 - \mathbf{x}|) \overleftrightarrow{\nabla}_x J_{m_2}(|\mathbf{x} - \mathbf{r}_2|) \\ &+ [\gamma J_{m_1}(|\mathbf{r}_1 - \mathbf{x}|) \overleftrightarrow{\nabla}_x J_{m_1}(|\mathbf{x} - \mathbf{r}_2|) \\ &+ \delta J_{m_2}(|\mathbf{r}_1 - \mathbf{x}|) \overleftrightarrow{\nabla}_x J_{m_2}(|\mathbf{x} - \mathbf{r}_2|)]\boldsymbol{\sigma}_1 \cdot \boldsymbol{\sigma}_2]. \quad (35) \end{aligned}$$

It is a simple task to prove that this current fulfills the continuity equation (23) with the Malfliet-Tjon potential in Eq. (24). For later purpose we list also the Fourier transform of the above MEC

$$\begin{aligned} \mathbf{j}_{(2)}^{\text{MTI-III}}(\mathbf{q}, \mathbf{r}_1, \mathbf{r}_2) &= \frac{e^{i\mathbf{q} \cdot \mathbf{R}}}{\pi^2}(\boldsymbol{\tau}_1 \times \boldsymbol{\tau}_2)_3\{\alpha \nabla_{\mathbf{r}} I_{m_1}(\mathbf{q}, \mathbf{r}) \\ &+ \beta \nabla_{\mathbf{r}} I_{m_2}(\mathbf{q}, \mathbf{r}) + \boldsymbol{\sigma}_1 \cdot \boldsymbol{\sigma}_2 \\ &\times [\gamma \nabla_{\mathbf{r}} I_{m_1}(\mathbf{q}, \mathbf{r}) + \delta \nabla_{\mathbf{r}} I_{m_2}(\mathbf{q}, \mathbf{r})]\}, \quad (36) \end{aligned}$$

where  $\mathbf{r}$  and  $\mathbf{R}$  denote relative and center-of-mass coordinates of the two-body subsystem, respectively, defined as

$$\mathbf{r} = \mathbf{r}_1 - \mathbf{r}_2 \quad \text{and} \quad \mathbf{R} = \frac{1}{2}(\mathbf{r}_1 + \mathbf{r}_2),$$

and

$$\begin{aligned} I_{m_{1/2}}(\mathbf{q}, \mathbf{r}) &= \int d^3p \frac{e^{i\mathbf{r} \cdot \mathbf{p}}}{[(\mathbf{p} + \frac{1}{2}\mathbf{q})^2 + m_{1/2}^2][(\mathbf{p} - \frac{1}{2}\mathbf{q})^2 + m_{1/2}^2]}. \quad (37) \end{aligned}$$

Here, we note that in contrast to a pseudoscalar meson exchange current the current in Eq. (36) does not include any contact term, but only meson in flight contributions, due to the fact that the MTI-III potential represents the exchange of scalar mesons. The functions  $I_{m_{1/2}}$  contain, in fact, the propagators of scalar mesons with effective masses  $m_1$  and  $m_2$  (for details see Ref. [25]).

### III. RESULTS AND DISCUSSION

Now, we present results for the longitudinal and transverse electric and magnetic response functions for  $^4\text{He}$ . We have solved the LIT equation (4) by using an expansion of the internal wave functions in terms of hyperspherical harmonics (HH). For the antisymmetrization we have used the powerful algorithm developed by Barnea and Novoselsky [26]. The HH expansion has been truncated beyond a maximum value  $K_{\text{max}}$  of the HH grand-angular momentum. Furthermore, the convergence of the HH expansion has been improved considerably by introducing the above-mentioned effective interaction with hyperspherical harmonics (EHHH-approach) [27], where the original bare potential has been replaced by an effective potential constructed via the Lee-Suzuki method [28]. When convergence is reached, the results agree with the ones obtained with the bare potential [27]. As original potential we have used the Malfliet-Tjon MTI-III potential [17]. We



found that for the ground state good convergence is reached with  $K_{\text{max}} = 10$ , yielding a binding energy of  $E_0 = -30.57$  MeV (the small difference with respect to the previously published value in [27] is due to the different  $K_{\text{max}}$  used). For the state  $\tilde{\Psi}_{\sigma,q}^{\mathcal{O}}$  of Eq. (3) we have used  $K_{\text{max}} = 11$  or 12 depending on the odd or even parity of the excitation operator  $\mathcal{O}$ , respectively. The results we are presenting are fully converged in  $K_{\text{max}}$ . We begin the discussion with the longitudinal response function.

### A. The longitudinal response function

Because the longitudinal response function is an incoherent sum of the separate multipole contributions it is useful to expand the charge operator into Coulomb multipoles as defined in Eq. (8). For each multipole operator the LIT equation with  $\mathcal{O}(q) = C_{\mu}^J(q)$  is solved. In view of the fact that isospin is a good quantum number and that the ground state of  $^4\text{He}$  has total isospin zero, one can treat the isoscalar and isovector parts of the charge operator separately. The multipole expansion has been truncated at a maximum value  $J_{\text{max}}$  determined by the requirement that convergence is achieved. It is known that with increasing momentum transfer  $J_{\text{max}}$  has to be increased too in order to reach convergence.

In Fig. 1, we present the response functions of the isovector multipoles, obtained from the inversion of the LIT of each multipole, as a function of the intrinsic energy  $\omega_{\text{int}} = E_f - E_0$ . We show results for two momentum transfers,  $q = 300$  and  $500$  MeV/c. One readily notes that for the lower-momentum

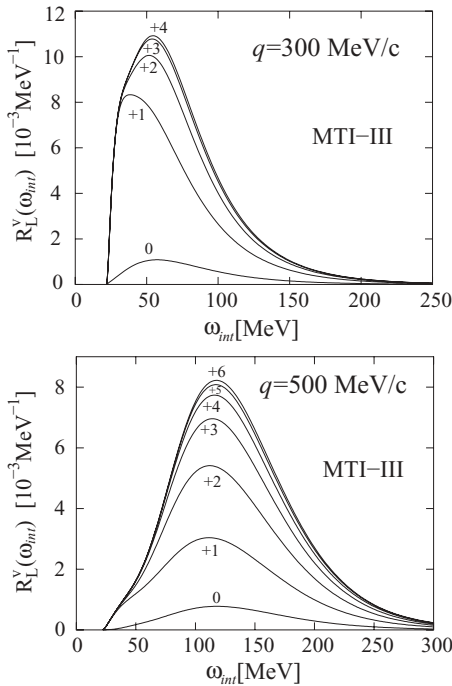


FIG. 1. Response functions of the lowest isovector Coulomb multipoles, starting with the monopole and consecutively adding higher multipoles up to  $J_{\text{max}} = 4$  for  $q = 300$  MeV/c (upper panel) and  $J_{\text{max}} = 6$  for  $q = 500$  MeV/c (lower panel), as a function of the intrinsic energy.

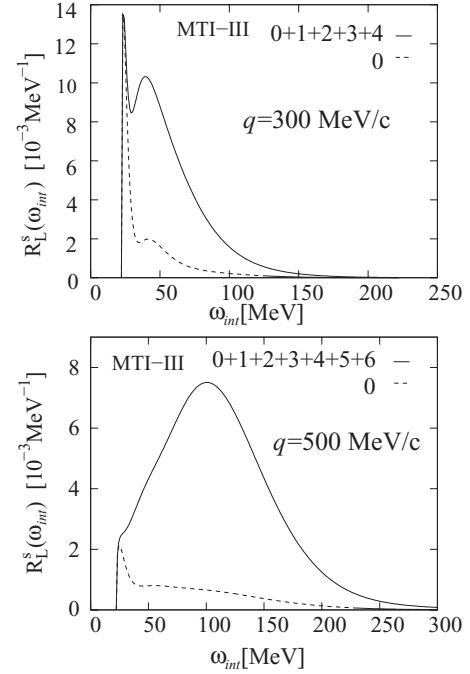


FIG. 2. The response functions of the isoscalar Coulomb monopole and the summed multipoles up to  $J_{\text{max}} = 4$  for  $q = 300$  MeV/c (upper panel) and  $J_{\text{max}} = 6$  for  $q = 500$  MeV/c (lower panel) as a function of the intrinsic energy.

transfer five multipoles are sufficient to reach convergence, whereas for the higher-momentum transfer two additional multipoles need to be included. The dominant feature is the quasi-elastic peak located at  $\omega_{\text{int}} \approx q^2/2m$ , where  $m$  is the mass of the nucleon, with a shoulder on the low energy side. The latter decreases rapidly with increasing momentum transfer.

The corresponding isoscalar response functions are displayed in Fig. 2. The contributions of the isoscalar monopole and of the sum of all multipoles up to  $J_{\text{max}}$  are shown separately. An interesting feature of the monopole is the pronounced peak close to threshold that is even higher than the quasi-elastic peak for the lower momentum transfer, but suppressed for the higher momentum transfer, although still visible as a shoulder. To better determine the width of the monopole excitation of  $^4\text{He}$  a more detailed study of low- $q$  transitions with a realistic nuclear interaction is necessary.

After the inclusion of the nucleon form factors and summing up the isoscalar and isovector contributions, we obtain the total longitudinal response function for varying energy transfers in the laboratory frame, where the recoil energy of the nucleus has been included. In Fig. 3, we compare our results with the available experimental data for momentum transfers  $q = 300$  and  $500$  MeV/c. We have taken into account the Darwin-Foldy lowest-order relativistic correction of the one-body charge density by a proper modification of the nucleon charge form factor [31]. Although the correction is negligible for  $q = 300$  MeV/c, it leads to a damping of about 6% of the total longitudinal strength in the quasi-elastic peak for  $q = 500$  MeV/c. The less important spin-orbit relativistic correction has been neglected (see, e.g., Ref. [10]).

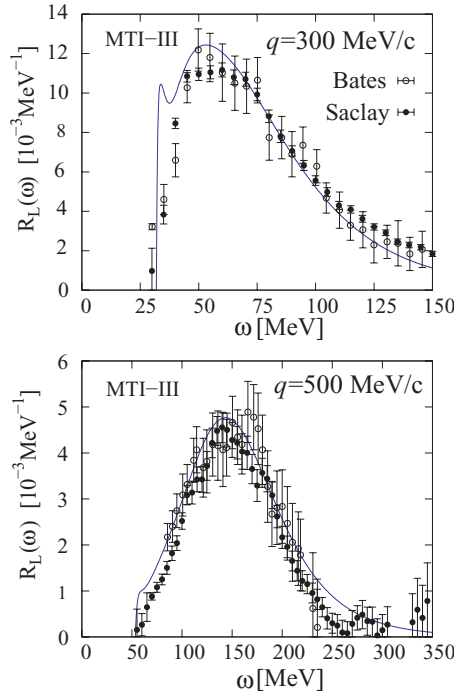


FIG. 3. (Color online) Longitudinal response function with the MTI-III potential as function of the energy for momentum transfers  $q = 300$  MeV/c (upper panel) and  $500$  MeV/c (lower panel). Experimental data from MIT-Bates [29] (open circles) and Saclay [30] (filled circles).

As in the previous calculation of  $R_L$  using the Trento (TN) potential [12], one notes that a semirealistic interaction, in this case the MTI-III, leads to quite a good overall description of the response in comparison to the experimental data from Bates [29] and Saclay [30].

The only difference to the previous calculation with the TN potential is the pronounced peak close to threshold in case of  $q = 300$  MeV/c that originates from the monopole excitation of  $^4\text{He}$ . However, such a peak is not seen in the data. But it is not clear whether the experimental energy resolution was sufficient to resolve such a structure. It is worthwhile to mention that a  $0^+$  resonance at  $20.10 \pm 0.05$  MeV with a width of  $270 \pm 50$  keV was determined in an electron-scattering experiment at momentum transfers  $q < 100$  MeV/c [32]. Here we do not calculate these low- $q$  kinematics, the resonance is very close to the “quasi-elastic peak” and quite small in size in comparison. A much more detailed study than the present calculation would be necessary to resolve such a rather complicated low-energy structure.

## B. The transverse response function

As done for the charge operator, we have expanded the transverse current operator into electric and magnetic multipoles according to Eqs. (12) and (13), separating them further into isoscalar and isovector parts, because the response function is an incoherent sum of these various multipole contributions. As discussed above, the transverse current includes one- and two-body operators. We first consider the one-body current alone, i.e., the spin and the convection current of Eq. (21). Later we add the consistent two-body current.

### 1. One-body current

It is known from standard PWIA calculations, that the spin current dominates the transverse response function at medium momentum transfers in the region of the quasi-elastic peak. Therefore, we start the discussion of the transverse response function of the spin current alone. In Fig. 4, we present the isoscalar and isovector response functions of the magnetic and

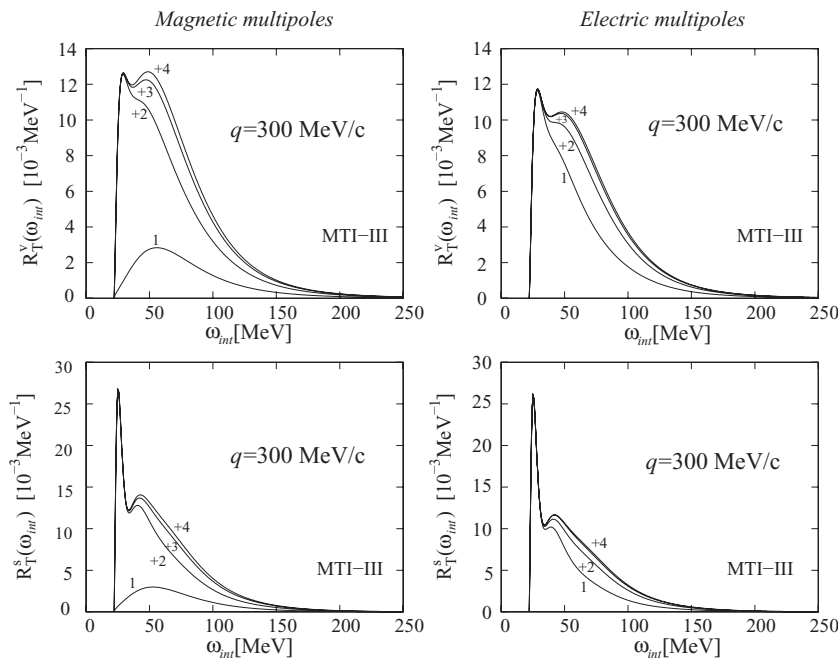


FIG. 4. Transverse response functions at  $q = 300$  MeV/c as functions of the intrinsic energy of various isovector (upper panels) and isoscalar (lower panels) magnetic (left) and electric (right) multipoles of the spin current, starting with the dipole and consecutively adding higher multipoles up to  $J_{\max} = 4$ .

electric multipoles up to  $J_{\text{max}} = 4$  for the spin current at a momentum transfer  $q = 300$  MeV/c. One readily notes that the dominant isovector contribution exhibits a substructure in the quasi-elastic peak region, which originates mainly from the magnetic quadrupole and electric dipole contributions. A very pronounced peak is also found in the magnetic and electric isoscalar responses close to threshold, which is, however, suppressed in relation to the isovector part of the total response function after the inclusion of the nucleon form factors, because of the smallness of the isoscalar magnetic form factor relative to the isovector one.

The second contribution of the one-body current to the transverse response function is given by the convection current of Eq. (21). In this case one has a derivative term caused by the dependence on the nucleon momentum  $\mathbf{p}_k$  in the anticommutator, which acts on the wave function. In the EIHH approach this derivative can be calculated analytically, due to the fact that the radial wave function is given in terms of Laguerre and Jacobi polynomials with hyperradial and hyperspherical variables, respectively (see Ref. [27]). To prove the correct implementation of the derivative term, we make use of the Siegert operator as a check. First, we write the convection current in momentum space as

$$\mathbf{j}_{(1)}^c(\mathbf{q}) = \mathbf{j}_{(1)}^{c,a}(\mathbf{q}) + \mathbf{j}_{(1)}^{c,b}(\mathbf{q}), \quad (38)$$

where

$$\mathbf{j}_{(1)}^{c,a}(\mathbf{q}) = \frac{e\mathbf{q}}{4m} \sum_k (1 + \tau_k^3) e^{i\mathbf{q} \cdot \mathbf{r}_k}, \quad (39)$$

$$\mathbf{j}_{(1)}^{c,b}(\mathbf{q}) = \frac{e}{2m} \sum_k (1 + \tau_k^3) e^{i\mathbf{q} \cdot \mathbf{r}_k} \mathbf{p}_k. \quad (40)$$

In this way, the first part  $\mathbf{j}_{(1)}^{c,a}(\mathbf{q})$  contains no derivative term and is purely longitudinal, whereas the second part  $\mathbf{j}_{(1)}^{c,b}(\mathbf{q})$  contains a longitudinal and a transverse term, depending on the direction of  $\mathbf{p}_k$  with respect to  $\mathbf{q}$ . The check consists in the comparison of the Siegert operator of Eq. (18) with the operator in Eq. (16) using the convection current of Eq. (38). For the case of a purely central potential, where no meson exchange currents are present, the two contributions have to coincide. As such an interaction we take for a test the model MTV', a modified version of the central Malfliet-Tjon-V, as defined in Ref. [24].

The results of this check for the dipole response are exhibited in Fig. 5 for different momentum transfers. First, one can note that the dipole strength is differently distributed depending on the momentum transfer: for the two lower  $q$  values the response function has a pronounced and quite small peak located a few MeV above threshold, whereas for the highest momentum transfer,  $q = 300$  MeV/c, the peak becomes considerably broader, but smaller in height and shifted to higher energies. This different behavior has its origin in a different dependence of the two contributions,  $\mathbf{j}_{(1)}^{c,a}(\mathbf{q})$  and  $\mathbf{j}_{(1)}^{c,b}(\mathbf{q})$ , to Eq. (16) on the momentum transfer. The current  $\mathbf{j}_{(1)}^{c,b}(\mathbf{q})$  is dominant at  $q = 3$  MeV/c, whereas for the two higher  $q$  values the second component,  $\mathbf{j}_{(1)}^{c,a}(\mathbf{q})$ , also becomes sizable and interferes constructively with  $\mathbf{j}_{(1)}^{c,a}(\mathbf{q})$  at  $q = 100$  MeV/c but destructively at  $q = 300$  MeV/c. However, their

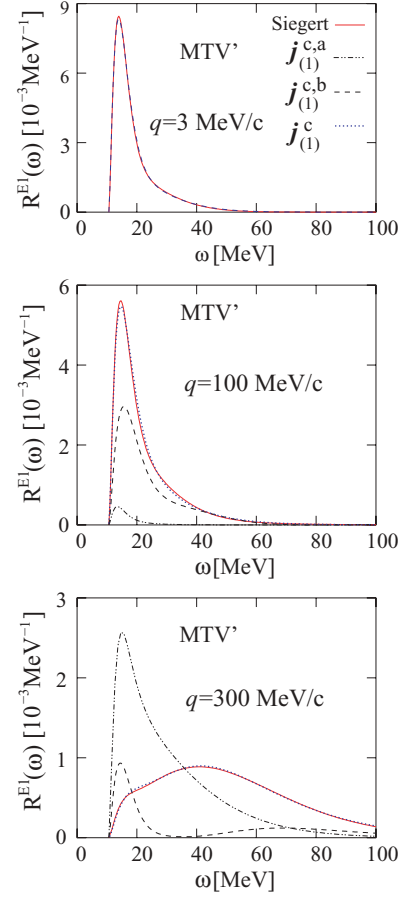


FIG. 5. (Color online) Siegert part of the dipole response function for different values of the momentum transfer and evaluated with (i) the Siegert operator of Eq. (18) and (ii) the operator of Eq. (16) with the convection currents  $\mathbf{j}_{(1)}^{c,a}(\mathbf{q})$  and  $\mathbf{j}_{(1)}^{c,b}(\mathbf{q})$ , and their sum (see text) for the MTV' potential.

total contribution agrees perfectly well with the Siegert dipole response.

Again, the convection current is expanded into electric and magnetic multipoles, and then the response function is calculated for each multipole until convergence is reached. For example, in case of medium momentum transfers like  $q = 300$  MeV/c we obtain a rather fast convergence pattern with  $J_{\text{max}} = 4$ , because only the dipole and quadrupole contributions cover about 80% of the total strength of the convection current. We also observe that only the electric multipoles are relevant, whereas the magnetic multipoles are negligible. For example, in case of  $q = 300$  MeV/c, the magnetic dipole induced by the convection current is 10 times smaller than the electric dipole.

Summing up the total contributions of spin and convection currents, we obtain the transverse response function in impulse approximation. In Fig. 6, we present the results for the MTI-III potential in comparison to the experimental data from Bates [30] and Saclay [32] for momentum transfers  $q = 300$  and  $500$  MeV/c. We also show the response given by the spin current only, which clearly dominates for both values of momentum transfer. For  $q = 300$  MeV/c the addition of the convection current produces an enhancement of 3–4% near

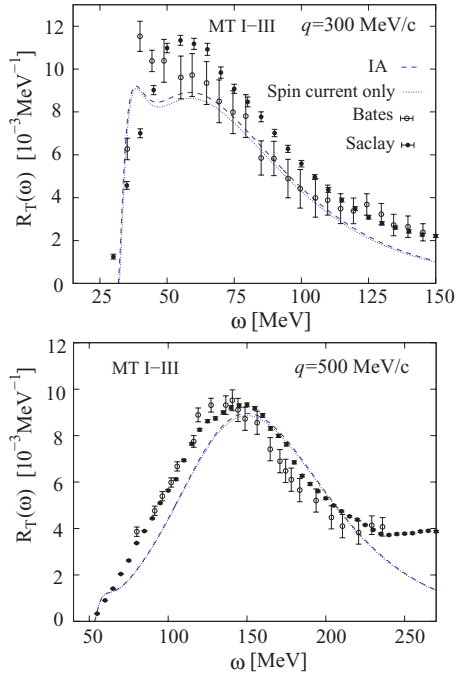


FIG. 6. (Color online) Transverse response function in impulse approximation (IA) and response of the one-body spin current alone as a function of the energy for momentum transfer  $q = 300$  (upper panel) and  $q = 500$  MeV/c (lower panel) in comparison with data from Bates [29] and Saclay [30].

the peak energy  $\omega = 60$  MeV. In case of  $q = 500$  MeV/c, the convection current contribution is negligible. Qualitatively, the IA results reproduce the position and the width of the quasi-elastic peak, but show some deviations in detail. For example, for  $q = 300$  MeV/c in the region of the maximum and above the theory is systematically below the data: in the maximum it is about 10% lower compared to the Bates data and 20% with respect to the Saclay data. On the low energy side the theory exhibits a steeper rise than the data and in addition a secondary maximum that is not seen in the Saclay data but might possibly be indicated by the Bates data. We point out that evidence for an  $M2$  resonance at 24 MeV was found in the above-mentioned  $(e, e')$  experiment [33]. However, for  $q = 500$  MeV/c, the theoretical height of the quasi-elastic peak is only about 5% lower with respect to experiment, but the peak position is shifted by about 6 MeV toward higher energies. Furthermore, the theoretical shoulder near the threshold is barely seen in the data. These substructures at low energies arise from the electric dipole and magnetic quadrupole contributions of the spin current.

It is conceivable that the overall missing strength could be provided by the up to now neglected two-body currents. Another explanation could be related to some inadequacies of the semirealistic description of the nuclear Hamiltonian or to relativistic effects. In the following subsection we will investigate the first possibility.

## 2. Two-body current

The consistent two-body current for the MTI-III potential,  $j_{(2)}^{\text{MTI-III}}(\mathbf{q}, \mathbf{r}_1, \mathbf{r}_2)$  is given in Eq. (36). Its general multipole

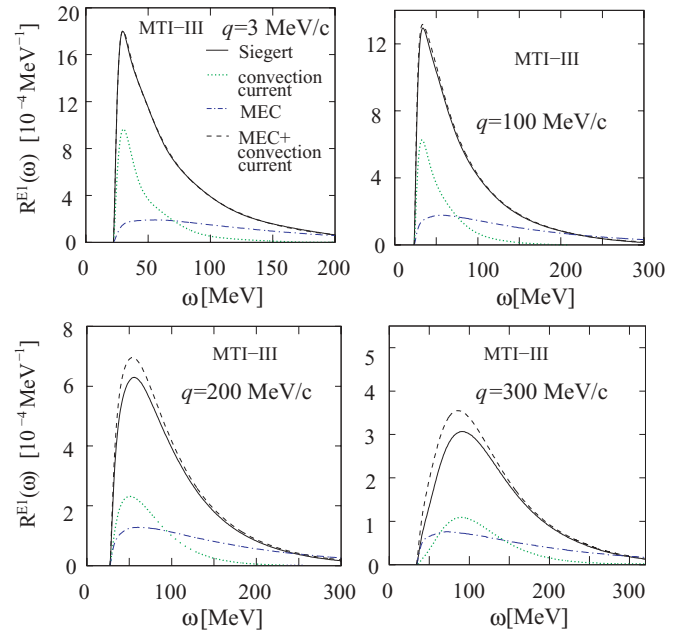


FIG. 7. (Color online) Dipole response function with the MTI-III potential, as a function of the energy and for different values of the momentum transfer. The response is evaluated for (i) the Siegert operator of (18) (solid curves) and for the operator of (16) with (ii) convection current (dotted), (iii) MEC (dash-dotted), and (iv) their sum (dashed).

decomposition is listed in Eq. (A10) of the appendix. In the present MEC calculation we neglect the center-of-mass motion of the two-body subsystem, i.e., we set  $e^{i\mathbf{q}\cdot\mathbf{R}} = 1$ . We point out that in this approximation all magnetic and even electric multipoles vanish identically (see the appendix). One expects this approximation to be quite good for small-momentum transfers, i.e.,  $qR \leq 1$ . In Fig. 7, we compare, for the most important dipole contribution, results with explicit MEC and convection current on the one hand and with the Siegert operator on the other hand.

In contrast to the MTV case depicted in Fig. 5 with the MTI-III potential, the Siegert dipole does not agree with the response of the Siegert part of the convection current alone, due to the presence of the MEC. At low momentum transfer the convection current leads to a response, whose peak height is only about half of the Siegert peak, whereas at higher momentum transfer the effect of MEC becomes even stronger. The dipole response function of the MEC is also shown in Fig. 7. It is interesting to note that the strength of the convection current is located near the quasi-elastic region, whereas the MEC has a much broader distribution. Taking as excitation operator the sum of convection current and MEC, we get a perfect agreement with the Siegert dipole for  $q = 3$  MeV/c, which clearly proves that the approximation introduced in the two-body current is reliable at low-momentum transfer, as expected. For  $q = 100$  MeV/c our approximation can still be considered very good. However, at the higher values of momentum transfer, one notes an increasing difference between the two evaluations that has to be assigned to the neglected center-of-mass motion of the two-body subsystems



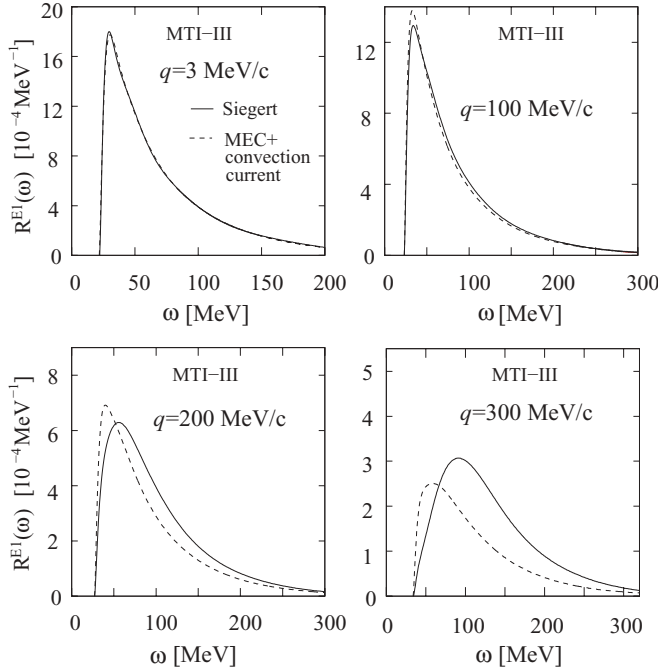


FIG. 8. Dipole response function with the MTI-III potential as a function of the energy for different values of the momentum transfer. The response is evaluated for (i) the Siegert operator of (18) (solid) and (ii) for total dipole operator according to Eq. (15) with the sum of convection current with MEC (dashed).

in the calculation of the MEC. One further observes that the effect of the approximation consists mainly in an enhancement of the peak height of the response, whereas position and form of the peak are not affected. The peak reduction amounts to about 10 and 20% for  $q = 200$  and  $300$  MeV/c, respectively.

Furthermore, we can check to what extent the Siegert operator alone is a good estimate of the total dipole operator, i.e., whether the correction term of Eq. (17) can safely be neglected. To this purpose we consider the total multipole of Eq. (15), where the correction term (17) has been included in addition to the Siegert part (16), and we compare it to the Siegert operator itself alone. In Fig. 8, we show the result of this check again for the isovector dipole response as a function of the energy for different momentum-transfer values. The total dipole response function induced by the convection current and by the MEC with mutual interference leads to the same result as the Siegert dipole response for the very low momentum transfer  $q = 3$  MeV/c, and even up to a momentum transfer of  $q = 100$  MeV, the Siegert operator is still a reliable approximation. This is no longer the case at higher momentum transfers where one readily notes an increasing difference between the total dipole response and the Siegert one alone. For momentum transfers  $q = 200$  and  $300$  MeV/c, the Siegert operator clearly underestimates the total dipole response at energies below the peak and overestimates it in the tail. In fact, the strength of the Siegert response is moved as a whole toward higher energies with a shift of the peak position with respect to the total dipole response by about 17 and 33 MeV for  $q = 200$  and  $300$  MeV/c, respectively. However, with respect to the total dipole response the peak height of the

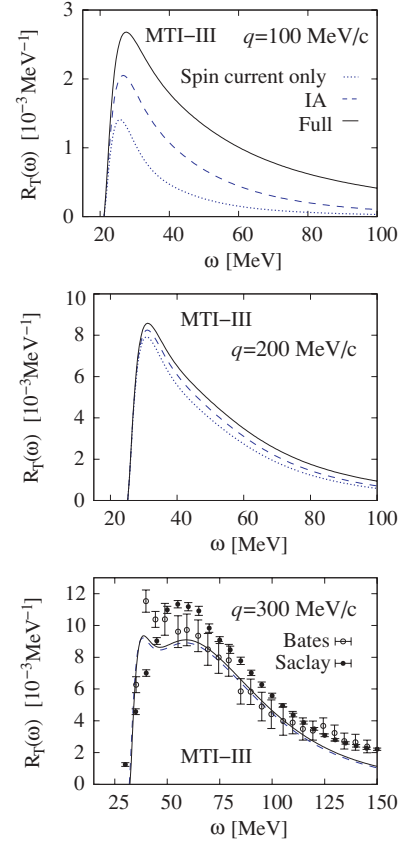


FIG. 9. (Color online) Transverse response function for different momentum transfer values: spin current only, IA, and full calculation with the inclusion of a consistent two-body current, in comparison with the available experimental data from Bates [29] and Saclay [30]. (For  $q = 300$  MeV/c the result for the spin current only is shown in Fig. 6).

Siegert response is reduced by about 10% at  $q = 200$  MeV/c and enhanced by about 20% for  $q = 300$  MeV/c. Obviously, the Siegert operator is not a good approximation for the total dipole response for  $q > 100$  MeV/c. At  $\omega = 100$  MeV, for example, compared to the result of the total dipole response, the Siegert response leads to an overestimation of 35% and 70% for  $q = 200$  and  $300$  MeV/c, respectively.

Though the situation may be quite different for other electric multipoles, like quadrupole and octupole, and even more for the isoscalar multipoles, we think that the results of this check on the dominant isovector dipole clearly suggests that one needs to consider the total electric multipoles when investigating the transverse response function at medium to high-momentum transfers, because in this kinematic region the Siegert approximation is no longer reliable. Thus, an explicit knowledge of the two-body current operator is necessary.

In Fig. 9, we finally present the transverse response function for different momentum transfers in comparison to the available experimental data. We compare the IA with the full calculation in which we add the two-body currents. For  $q = 100$  and  $200$  MeV/c we also show the response function induced by the spin current only. In Table I, we recall explicitly the multipoles considered in our final calculations of  $R_T(\omega, q)$  for the different transverse current parts and for

TABLE I. Maximal multipolarity  $J_{\max}$  considered in the calculation shown in Fig. 9 for the one- and two-body currents and for the different momentum-transfer values.

$q$ (MeV/c)	$J_{(1)}(q)$	$J_{(2)}(q)$
100	2	1
200	3	1
300	4	3

each momentum transfer value. As previously shown in Fig. 6, the spin current strongly dominates the response function at a momentum transfer  $q = 300$  MeV/c. A rather similar situation is found for  $q = 200$  MeV, as depicted in Fig. 9. However, one can see that for the lower momentum transfer  $q = 100$  MeV/c the convection current presents a stronger effect: for example, at  $\omega = 40$  MeV it is even half of the total IA strength. By comparing the IA with the full calculation, we can conclude that quite a strong effect of the MEC is found at low momentum transfers like for  $q = 100$  MeV, where, for example, at energies of 100 MeV they lead to an enhancement of the strength by a factor of 4 with respect to the IA. At this momentum transfer, the approximation we had introduced for the MEC is safely reliable. As the momentum transfer increases, for example, at  $q = 200$  MeV/c, the enhancing effect of the MEC with respect to the IA result on  $R_T$  is reduced dramatically and amounts to only 4% in the peak region and to 40% for  $\omega = 100$  MeV. Unfortunately, to the best of our knowledge, no experimental data have been measured in the quasi-elastic region at these low momentum transfers  $q = 100$  and 200 MeV/c. For the case of  $q = 300$  MeV/c where experimental data from Bates [29] and Saclay [30] exist, we observe a tiny effect of the two-body current with respect to IA result. The addition of the MEC leads to an increase of 4% and almost 10% at  $\omega = 100$  and 150 MeV, respectively. Our full calculation agrees rather well with the data of Bates in

the energy range  $55 \leq \omega \leq 115$  MeV but is lower than the data of Saclay in the quasi-elastic peak region and above. For example, at  $\omega = 60$  MeV our full result for  $q = 300$  MeV/c is still lower than the measurement of Saclay.

Here we mention that the approximation introduced in the MEC by neglecting the center-of-mass dependence, which is estimated to be of about 10 to 20% in the peak and negligible in the tail for  $q = 200$  to 300 MeV/c, does not affect our conclusion, due to the fact that the overall MEC effect is small.

#### IV. CONCLUSIONS AND OUTLOOK

We have presented the first calculation of the inclusive longitudinal and transverse response functions of  $^4\text{He}$  within the LIT and EIHH methods with complete inclusion of the interaction in the final states as given by the semirealistic potential MTI-III potential. As in previous LIT calculations with the semirealistic TN potential [12] a good overall agreement with available experimental data is found for the longitudinal response function, though the MTI-III potential leads in addition to the quasi-elastic peak to another peak close to threshold, which is not clearly seen in the data of Bates [29] and Saclay [30], whereas, as mentioned, at  $q < 100$  MeV/c a resonance close to threshold has been observed in experiment [32].

For the transverse response function, we have performed a calculation in IA alone and then adding in a second step a two-body current consistent with the MTI-III potential. Strong MEC effects are found at low momentum transfer,  $q = 100$  MeV/c, where unfortunately no experimental data are available. For the case of  $q = 300$  MeV/c, for which data from Bates [29] and Saclay [30] exist, we have shown that the IA result still misses some strength in the quasi-elastic peak region. For the present MEC, consistent to the semirealistic potential model, we have not found a strong two-body current effect at  $q = 300$  MeV/c as obtained in the calculation of Carlson and Schiavilla within the Laplace transform approach [16], including  $\pi$ - and  $\rho$ -MEC. A direct comparison of the two calculations for  $R_T(\omega, q)$  is not possible because the inversion of the Laplace transform suffers from large instabilities. In Fig. 10, we thus compare the Laplace transform of our full transverse response function for  $q = 300$  MeV/c with the GFMC Euclidean response, using as interaction the Argonne V18 potential [33] with the addition of the Urbana IX three-body force [34]. We adopt the definition of the Euclidean response as presented in Refs. [15,16] and we integrate our theoretical curve up to the maximal value of energy transfer ( $\omega_{\max} = 180$  MeV) measured in Saclay [30] for the considered momentum transfer case. Consistently with what is obtained in a direct comparison, our calculation for the MTI-III potential with the present MEC model leads to a lower transverse Euclidean response with respect to the Laplace transform of experimental data. The Euclidean response obtained with the GFMC, where contributions of  $\pi$ - and  $\rho$ -exchange currents were considered, agrees better with data. Obviously, the additional contribution of the present MEC does not explain the missing strength of our model. The reason for our relatively

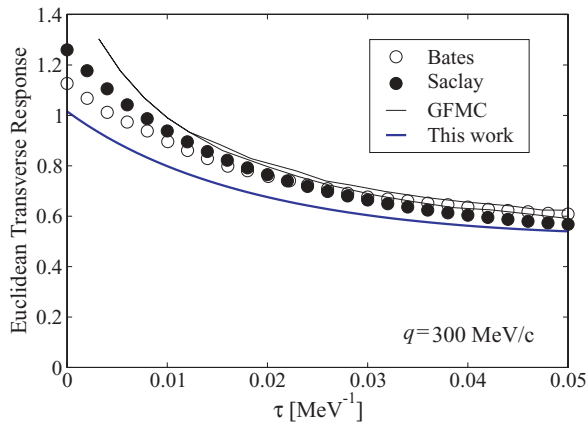


FIG. 10. (Color online) Euclidean transverse response for momentum transfer  $q = 300$  MeV/c. Comparison of the GFMC calculation [16] (band between thin lines) and the result of this work (thick line) with the Laplace transform of experimental data from Bates [29] and Saclay [30].

small MEC contribution lies in the fact that our potential model comprises solely fictitious scalar mesons and misses explicit pionic degrees of freedom. Consequently, the corresponding MEC includes no contact terms that are known to be important in the  $\pi$ -MEC. Moreover, the masses of the exchanged mesons of the present potential model are considerably higher than the pion mass making the exchange current shorter ranged and thus less important in the range of momentum transfers considered in this work. Thus it might not be surprising that we find a reduced effect of MEC. In view of these findings we have to conclude that very likely the major difference to the GFMC calculation is due to the missing explicit pionic degrees of freedom in our potential model and, therefore, also in the corresponding MEC. For a better quantitative description of inclusive electron scattering off  $^4\text{He}$  the use of more realistic potentials and meson exchange currents, including pion degrees of freedom, is certainly important. The present work constitutes a first step toward this final aim, and a further extension of our methods is under consideration. In future studies with a longer ranged MEC one would also need to go beyond the present approximation of neglecting the two-body center-of-mass contribution (see Sec. III B2), limiting the present approach to not too high momentum transfers.

### ACKNOWLEDGMENTS

The authors S.B. and H.A. thank the Deutsche Forschungsgemeinschaft for partial support (SFB 443). This work was furthermore partially supported by the Israel Science Foundation (grant 361/05).

### APPENDIX: MULTIPOLE EXPANSION OF THE MEC

Here we give a brief derivation of the multipole expansion of a two-body current of the form

$$\mathbf{j}_{(2)}(\mathbf{q}, \mathbf{r}, \mathbf{R}) = e^{i\mathbf{q}\cdot\mathbf{R}} \tilde{\mathbf{j}}_{(2)}(\mathbf{q}, \mathbf{r}), \quad (\text{A1})$$

consisting of an intrinsic part  $\tilde{\mathbf{j}}_{(2)}$ , which depends only on the relative two-body coordinate  $\mathbf{r}$  and a two-body center-of-mass part, depending on the two-body center-of-mass coordinate  $\mathbf{R}$ . The consistent meson exchange current of Eq. (36) has exactly this form.

The basic quantities to evaluate are

$$J_{L,M}^J(\mathbf{q}, \mathbf{r}) = \frac{1}{4\pi} \int d\hat{q}' e^{i\mathbf{q}\cdot\mathbf{R}} \mathbf{Y}_{L,M}^J(\hat{q}') \cdot \nabla \tilde{\mathbf{j}}_{(2)}(\mathbf{q}', \mathbf{r}), \quad (\text{A2})$$

where  $\mathbf{Y}_{L,M}^J$  denotes a vector spherical harmonics. The quantities in Eq. (A2) determine the longitudinal and transverse electric and magnetic multipoles according to

$$L_0^J = -\sum_L (-)^L \hat{L} \begin{pmatrix} L & 1 & J \\ 0 & 0 & 0 \end{pmatrix} J_{L,0}^J, \quad (\text{A3})$$

$$T_\mu^{el,J} = -\sqrt{2} \sum_{L=J\pm 1} (-)^L \hat{L} \begin{pmatrix} L & 1 & J \\ 0 & 1 & -1 \end{pmatrix} J_{L,\mu}^J, \quad (\text{A4})$$

$$T_\mu^{\text{mag},J} = -\sqrt{2} (-)^J \hat{J} \begin{pmatrix} J & 1 & J \\ 0 & 1 & -1 \end{pmatrix} J_{J,\mu}^J = J_{J,\mu}^J, \quad (\text{A5})$$

for  $|\mu| = 1$ . Here a spherical coordinate system  $\epsilon_\mu$  with  $\mu \in \{0, \pm 1\}$  has been chosen where  $\epsilon_0$  is along  $\mathbf{q}$ . For more details the reader should consult Ref. [24].

To evaluate Eq. (A2) one first expands  $e^{i\mathbf{q}\cdot\mathbf{R}}$  and the intrinsic current  $\tilde{\mathbf{j}}_{(2)}(\mathbf{q}, \mathbf{r})$  into spherical harmonics. The former one is given by the well known expression

$$e^{i\mathbf{q}\cdot\mathbf{R}} = 4\pi \sum_{J_R} (-)^{J_R} \hat{J}_R [C^{J_R}(\mathbf{q}, \mathbf{R}) \times Y^{J_R}(\hat{\mathbf{q}})]^0, \quad (\text{A6})$$

where we have introduced the center-of-mass Coulomb multipoles

$$C^{J_R}(\mathbf{q}, \mathbf{R}) = i^{J_R} j_{J_R}(qR) Y^{J_R}(\hat{\mathbf{R}}), \quad (\text{A7})$$

with spherical Bessel functions  $j_l(x)$ . The corresponding expansion for the intrinsic current is given by

$$\tilde{\mathbf{j}}_{(2)}(\mathbf{q}, \mathbf{r}) = 4\pi \sum_{J_r, m_r, L_r} \tilde{J}_{L_r, m_r}^{J_r}(\mathbf{q}, \mathbf{r}) \mathbf{Y}_{L_r, m_r}^{J_r}(\hat{\mathbf{q}})^*, \quad (\text{A8})$$

where

$$\tilde{J}_{L_r, m_r}^{J_r}(\mathbf{q}, \mathbf{r}) = \frac{1}{4\pi} \int d\hat{q}' Y_{L_r, m_r}^{J_r}(\hat{q}') \cdot \nabla \tilde{\mathbf{j}}_{(2)}(\mathbf{q}', \mathbf{r}). \quad (\text{A9})$$

Inserting these expansions into Eq. (A2), then, after recoupling, the angular integration can be done analytically, and one finds finally

$$\begin{aligned} J_{L,\mu}^J(\mathbf{q}, \mathbf{r}, \mathbf{R}) &= (-)^{J+1} \sqrt{4\pi} \hat{J} \hat{L} \sum_{J_r, J_r, L_r} \hat{J}_R \hat{L}_r \begin{pmatrix} J_R & L_r & L \\ 0 & 0 & 0 \end{pmatrix} \\ &\times \left\{ \begin{matrix} J_R & J_r & J \\ 1 & L & L_r \end{matrix} \right\} [C^{J_R}(\mathbf{q}, \mathbf{R}) \times \tilde{J}_{L_r}^{J_r}(\mathbf{q}, \mathbf{r})]_\mu^J. \end{aligned} \quad (\text{A10})$$

With the help of angular momentum algebra, the longitudinal and transverse multipoles are then obtained from Eqs. (A3) through (A5), i.e.,

$$\begin{aligned} L_0^J(\mathbf{q}, \mathbf{r}, \mathbf{R}) &= (-)^J \frac{\sqrt{4\pi}}{\hat{J}} \sum_{J_R, J_r} \hat{J}_R^2 \hat{J}_r \begin{pmatrix} J_R & J_r & J \\ 0 & 0 & 0 \end{pmatrix} \\ &\times [C^{J_R}(\mathbf{q}, \mathbf{R}) \times \tilde{L}^{J_r}(\mathbf{q}, \mathbf{r})]_0^J, \end{aligned} \quad (\text{A11})$$

$$\begin{aligned} T_\mu^{el/\text{mag},J}(\mathbf{q}, \mathbf{r}, \mathbf{R}) &= (-)^{J+1} \frac{\sqrt{\pi}}{\hat{J}} \sum_{J_R, J_r} \hat{J}_R^2 \hat{J}_r \begin{pmatrix} J_R & J_r & J \\ 0 & -1 & 1 \end{pmatrix} \\ &\times (1 \pm (-)^{J_r+J_r+J}) [C^{J_R}(\mathbf{q}, \mathbf{R}) \\ &\times \tilde{T}^{el/\text{mag},J_r}(\mathbf{q}, \mathbf{r})]_\mu^J. \end{aligned} \quad (\text{A12})$$

Thus a total longitudinal or transverse multipole is given by a sum of all possible couplings of corresponding intrinsic and center-of-mass charge multipoles as allowed by parity and angular momentum coupling rules to form a rank- $J$  tensor.

With respect to the multipole expansion of the consistent MEC of Eq. (36) we start from the expansion  $\nabla I_m$ , which is given in [25]

$$\nabla I_m(\mathbf{q}, \mathbf{r}) = 4\pi \sum_{J_r \mu L_r = \text{even}} \tilde{I}_{L_r \mu}^{J_r}(\mathbf{q}, \mathbf{r}, m) \mathbf{Y}_{L_r \mu}^{J_r}(\hat{\mathbf{q}})^* \quad (\text{A13})$$

with

$$\tilde{I}_{L\mu}^J(\mathbf{q}, \mathbf{r}, m) = 4\pi(i)^{J-1} \hat{L} \begin{pmatrix} 1 & L & J \\ 0 & 0 & 0 \end{pmatrix} Y_\mu^J(\hat{\mathbf{r}}) \Phi_{J,L}^1(\mathbf{q}, \mathbf{r}, m), \quad (\text{A14})$$

where the functions  $\Phi_{\sigma,l}^v(\mathbf{q}, \mathbf{r}, m)$  are defined by

$$\Phi_{\sigma,\ell}^v(\mathbf{q}, \mathbf{r}, m) = \frac{1}{q^2} \int_0^\infty \frac{dpp^v}{z} j_\sigma(pr) Q_\ell(z), \quad (\text{A15})$$

with  $z = (p^2 + \frac{1}{4}q^2 + m^2)/pq$  and

$$Q_\ell(z) = \frac{1}{2} \int_{-1}^1 dx \frac{P_\ell(z)}{z-x}. \quad (\text{A16})$$

Here,  $P_\ell(z)$  denotes a Legendre polynomial. Then one obtains for the intrinsic part of the MEC in (36)

$$\begin{aligned} \tilde{J}_{L_r \mu}^{J_r}(\mathbf{q}, \mathbf{r}) &= \frac{4}{\pi} (\boldsymbol{\tau}_1 \times \boldsymbol{\tau}_2)_3 (i)^{J_r-1} \hat{L}_r \begin{pmatrix} 1 & L_r & J_r \\ 0 & 0 & 0 \end{pmatrix} Y_\mu^{J_r}(\hat{\mathbf{r}}) \\ &\times \{ \alpha \Phi_{J_r, L_r}^1(\mathbf{q}, \mathbf{r}, m_1) + \beta \Phi_{J_r, L_r}^1(\mathbf{q}, \mathbf{r}, m_2) \\ &+ \boldsymbol{\sigma}_1 \cdot \boldsymbol{\sigma}_2 [\gamma \Phi_{J_r, L_r}^1(\mathbf{q}, \mathbf{r}, m_1) \\ &+ \delta \Phi_{J_r, L_r}^1(\mathbf{q}, \mathbf{r}, m_2)] \}, \end{aligned} \quad (\text{A17})$$

which, inserted into Eqs. (A11) and (A12), finally yields the MEC multipoles. From the condition “ $L_r = \text{even}$ ” follows in conjunction with the  $3j$ -symbol in Eq. (A14) that  $\tilde{J}_{L_r}^{J_r}(\mathbf{q}, \mathbf{r})$  vanishes for  $L_r = J_r$  and consequently all intrinsic magnetic and even electric multipoles vanish according to Eqs. (A4) and (A5).

If one neglects the center-of-mass contributions, i.e., setting  $\mathbf{R} = 0$ , then one has

$$J_{L\mu}^J(\mathbf{q}, \mathbf{r}, \mathbf{0}) = \tilde{J}_{L\mu}^J(\mathbf{q}, \mathbf{r}). \quad (\text{A18})$$

This approximation is used in the present work.

- 
- [1] H. Kamada *et al.*, Phys. Rev. C **64**, 044001 (2001).
  - [2] V. D. Efros, W. Leidemann, and G. Orlandini, Phys. Lett. **B338**, 130 (1994).
  - [3] S. Bacca, M. A. Marchisio, N. Barnea, W. Leidemann, and G. Orlandini, Phys. Rev. Lett. **89**, 052502 (2002).
  - [4] S. Bacca, H. Arenhövel, N. Barnea, W. Leidemann, and G. Orlandini, Phys. Lett. **B603**, 159 (2004).
  - [5] D. Gazit, S. Bacca, N. Barnea, W. Leidemann, and G. Orlandini, Phys. Rev. Lett. **96**, 112301 (2002).
  - [6] D. Gazit and N. Barnea, Phys. Rev. C **70**, 048801 (2004).
  - [7] D. Gazit and N. Barnea, Phys. Rev. Lett. **98**, 192501 (2007).
  - [8] S. Quaglioni, W. Leidemann, G. Orlandini, N. Barnea, and V. D. Efros, Phys. Rev. C **69**, 044002 (2004).
  - [9] S. Quaglioni, V. D. Efros, W. Leidemann, and G. Orlandini, Phys. Rev. C **72**, 064002 (2005).
  - [10] V. D. Efros, W. Leidemann, G. Orlandini, and E. L. Tomusiak, Phys. Rev. C **69**, 044001 (2004).
  - [11] V. D. Efros, W. Leidemann, G. Orlandini, and E. L. Tomusiak, Phys. Rev. C **72**, 011002(R) (2005).
  - [12] V. D. Efros, W. Leidemann, and G. Orlandini, Phys. Rev. Lett. **78**, 432 (1997).
  - [13] V. D. Efros, W. Leidemann, and G. Orlandini, Phys. Rev. C **58**, 582 (1998).
  - [14] C. Ciofi degli Atti and S. Simula, Phys. Rev. C **53**, 1689 (1996).
  - [15] J. Carlson and R. Schiavilla, Phys. Rev. Lett. **68**, 3682 (1992).
  - [16] J. Carlson and R. Schiavilla, Phys. Rev. C **49**, R2880 (1994).
  - [17] R. A. Malfliet and J. A. Tjon, Nucl. Phys. **A127**, 161 (1969).
  - [18] V. D. Efros, W. Leidemann, and G. Orlandini, Few-Body Syst. **26**, 251 (1999).
  - [19] D. Andreasi, W. Leidemann, C. Reiß, and M. Schwamb, Eur. Phys. J. A **24**, 361 (2005).
  - [20] J. M. Eisenberg and W. Greiner, *Excitation Mechanisms of the Nucleus* (North-Holland, Amsterdam, 1970).
  - [21] S. Galster *et al.*, Nucl. Phys. **B32**, 221 (1971).
  - [22] D. O. Riska, Phys. Scr. **31**, 471 (1985).
  - [23] A. Buchmann, W. Leidemann, and H. Arenhövel, Nucl. Phys. **A443**, 726 (1985).
  - [24] S. Bacca, PhD thesis, Universities Mainz and Trento, 2005.
  - [25] W. Fabian and H. Arenhövel, Nucl. Phys. **A258**, 461 (1976).
  - [26] N. Barnea and A. Novoselsky, Ann. Phys. (NY) **256**, 192 (1997); Phys. Rev. A **57**, 48 (1998).
  - [27] N. Barnea, W. Leidemann, and G. Orlandini, Phys. Rev. C **61**, 054001 (2000); Nucl. Phys. **A693**, 565 (2001).
  - [28] K. Suzuki and S. Y. Lee, Prog. Theor. Phys. **64**, 2091 (1980).
  - [29] S. A. Dytman *et al.*, Phys. Rev. C **38**, 800 (1988).
  - [30] A. Zghiche *et al.*, Nucl. Phys. **A572**, 513 (1994).
  - [31] J. L. Friar, Ann. Phys. (N.Y.) **81**, 332 (1973); Nucl. Phys. **A264**, 455 (1976).
  - [32] Th. Walcher, Phys. Lett. **B31**, 442 (1970); Z. Phys. **237**, 368 (1970).
  - [33] R. B. Wiringa, V. G. J. Stoks, and R. Schiavilla, Phys. Rev. C **51**, 38 (1995).
  - [34] B. S. Pudliner, V. R. Pandharipande, J. Carlson, S. C. Pieper, and R. B. Wiringa, Phys. Rev. C **56**, 1720 (1997).